Growth of Polythiophene/Perylene Tetracarboxydiimide Donor/Acceptor Shish-Kebab Nanostructures by Coupled Crystal Modification

Laju Bu, Emily Pentzer, Felicia A. Bokel, Todd Emrick, and Ryan C. Hayward*

Department of Polymer Science and Engineering, University of Massachusetts, Amherst, Massachusetts 01003, United States

ABSTRACT Self-assembled crystalline organic nanostructures containing electron donor and acceptor materials hold promise as building blocks for photovoltaic devices. We show that coupled crystallization of poly(3-hexyl thiophene) (P3HT) and perylene tetracarboxydiimide (PDI) induced by solvent evaporation, wherein both components modify crystallization of the other, gives rise to donor/acceptor "shish-kebabs" with tunable nanostructures. P3HT kinetically stabilizes supersaturated solutions of PDI and modifies the growth of PDI crystals, leading to formation of extended PDI shish nanowires that in turn serve as heterogeneous nucleation sites for fibrillar P3HT kebabs during solvent casting. The dimensions of these nanostructures can be tailored through variations in donor/acceptor ratio or solvent quality, and the method is shown to be general to several other poly(3-alkyl thiophenes) and perylene derivatives, thus providing a simple and robust route to form highly crystalline nanophase separated organic donor/acceptor assemblies.

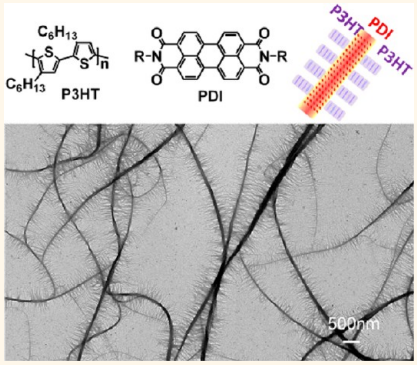

KEYWORDS: poly(3-hexyl thiophene) (P3HT) · perylene tetracaboxydiimide · donor/acceptor · shish-kebab cystals · coupled crystallization · heterogeneous nucleation

Exercising control over both the nanoscale morphology and crystalline packing of electron donor and acceptor materials within a single thin film is a key challenge in the design of organic photovoltaics.[1−3] The presence of distinct domains of both materials, with dimensions comparable to the exciton diffusion length, is critical for efficient charge separation, while crystalline ordering within each domain is important for promoting high charge carrier mobilities.[4,5] For bulk heterojunction devices based on physical blends of donors and acceptors, solvent or thermal annealing treatments have been used to improve molecular scale organization, and therefore device efficiency.[6] However, extended annealing can lead to undesired coarsening of domains[7] and thus an optimum in performance is typically seen for intermediate annealing treatments that balance crystallinity and phase separation. Macromolecules containing donors and acceptors covalently tethered to one another, as in block-copolymers[8] or co-oligomers,[9,10] can provide superior control over nanoscale morphology, since they fundamentally restrict the length scale over which phase separation can occur. However, the performance of these materials has so far remained far below the level of simple blends, at least in part because covalent attachment of the two materials typically places fundamental limits on how crystals of each material can form. Well designed supramolecular interactions can also facilitate coassembly of donor and acceptor materials,[11] for example through hydrogen bonding;[12−14] however, this route has been less extensively explored in the context of organic photovoltaics.

Using nanocrystals of one component to template crystallization of the other, either by epitaxial growth or heterogeneous nucleation, is a promising route to fabricate bicrystalline donor/acceptor nanostructures.[15,16] While heteroepitaxy of crystalline nanostructures is common for inorganic semiconductors,[17,18] there are relatively few

* Address correspondence to rhayward@mail.pse.umass.edu.

Received for review September 21, 2012 and accepted November 11, 2012.

Published online November 19, 2012
10.1021/nn3043836

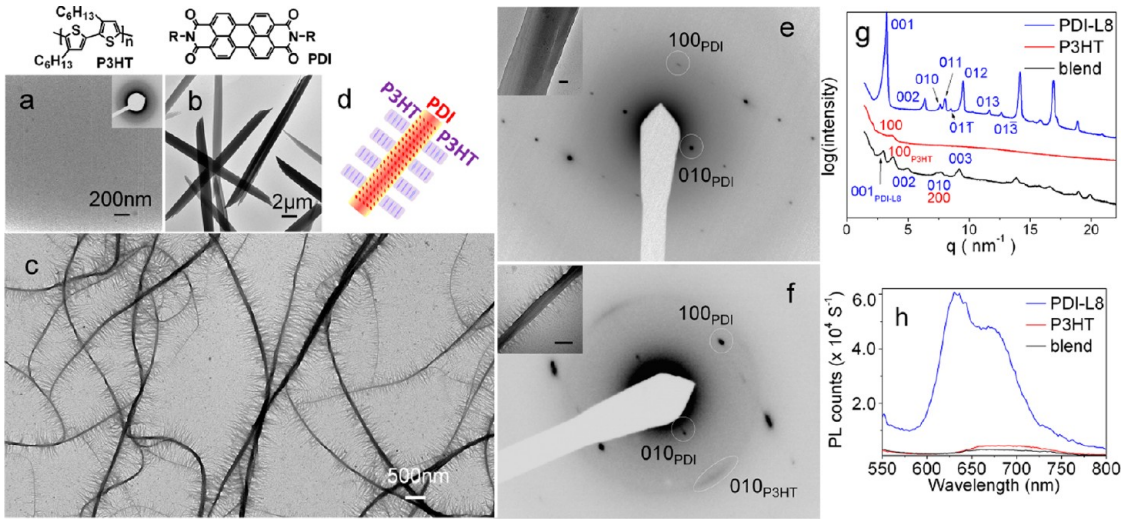

Figure 1. TEM (a−c), SAED (e,f), XRD (g), and photoluminescence (h) characterization of drop casted films of P3HT, PDI-L8, and blend solutions in ODCB. (a) A nearly featureless film with limited crystallinity obtained for a solution of 1 mg/mL P3HT alone (inset: SAED); (b) ribbon-like crystals formed from a metastable 0.5 mg/mL PDI-L8 solution; (c) shish-kebab hybrid crystals from a blend solution containing 1 mg/mL P3HT and 0.5 mg/mL PDI-L8; (d) a schematic of the shish-kebab structure. SAED of a PDI-L8 ribbon-like crystal (e) and a shish-kebab crystal (f) with their corresponding crystal images as insets, both scale bars are 200 nm. The red indices in the XRD pattern (g) are for P3HT, and blue for PDI.

examples for organic donors and acceptors,[19] likely due to the broad diversity of structures adopted by conjugated organic molecules and polymers.[20] Nonspecific heterogeneous nucleation, however, may represent a more general route for preparing crystalline organic heterostructures. For example, regioregular poly(3-hexyl thiophene) (P3HT), an extensively studied conjugated polymer donor, readily nucleates on surfaces of other materials,[21] including carbon nanotubes (CNT),[22] reduced graphene oxide,[23,24] 1,3,5-trichlorobenzene crystals,[25] potassium 4-bromobenzoate,[26] and preformed P3HT nanowires.[27−29]

In the current report, we investigate the formation of nanocrystalline structures that grow during solvent casting of blend solutions of P3HT with perylene tetracarboxy diimide (PDI) species. Derivatives of PDI are among the most promising electron accepting organic materials due to their high electron mobility, broad light absorption, and long-term environmental stability.[30] However, photovoltaic devices made using combinations of perylene derivatives and polythiophenes have generally shown relatively poor performance[31−37] for reasons that remain incompletely understood. We anticipate that approaches to tailor nanoscale crystalline structures of these materials may provide a route to enhance photovoltaic performance, or at least to enable fundamental studies of the relationships between nanocrystalline morphology and photophysical behavior.

We report here that solvent removal from blend solutions of P3HT and PDI leads to growth of hybrid "shish-kebab" nanostructures, each consisting of a PDI nanowire shish coated by fibrillar P3HT kebabs. We dub the mechanism of growth "coupled crystal modification", since P3HT and PDI both influence the crystallization behavior of each other. Specifically, P3HT serves as a soluble additive that kinetically inhibits the formation of PDI crystals from supersaturated solutions and also reduces their lateral dimensions. In turn, these P3HT-modified PDI nanocrystals serve as highly efficient nucleating agents for growth of P3HT fibers when P3HT becomes supersaturated during solvent casting. This process of coupled crystal modification not only enhances the crystallinity of the P3HT donor domains in cast films, but also allows the lateral dimensions of the PDI acceptor domains to be tuned from ∼200 nm down to 25 nm simply through changes in mixing ratio. The mechanism is shown to be general to several different organic solvents, and several polythiophene and perylene derivatives, thus providing a flexible means to control both nanoscale structure and crystalline ordering in these donor/acceptor blends.

RESULTS AND DISCUSSION

We first study the behavior of *N*,*N*′-dioctyl perylene diimide (PDI-L8) and P3HT (polystyrene equivalent $\bar{M}_w$ = 6 kg/mol, molar-mass dispersity $Đ_M$ = 1.20 from size exclusion chromatography; regioregularity, 94%) with 1,2-dichlorobenzene (ODCB) as a solvent. P3HT is highly soluble in ODCB, and drop casting of films from solutions containing only P3HT (1.0 mg/mL) yields nearly featureless films with a few crystalline nanofibers in the thicker regions of the film, as shown in Figure 1a by transmission electron microscopy (TEM), and the corresponding selected area electron diffraction (SAED) pattern, which contains only a broad diffuse diffraction ring at 0.38 nm, corresponding to the (010) spacing. The solubility of PDI-L8 in ODCB is much lower

(0.12 mg/mL at room temperature), but metastable solutions with higher concentration are prepared by heating to 75 °C for 10 min, followed by cooling to room temperature. Casting a supersaturated solution of PDI-L8 alone (0.5 mg/mL) within ~10 min of cooling to room temperature leads to growth of ribbon-like crystals with typical widths of ~2 μm and lengths of ~20 μm (as seen *via* TEM in Figure 1b), and thicknesses from 150 nm to 1 μm as measured by AFM (Supporting Information, Figure S1). These crystals are similar in shape to those formed at the chloroform/methanol interface,[38] though somewhat thicker and shorter.

Remarkably, casting a mixture of P3HT and PDI-L8 from ODCB leads to growth of shish-kebab crystal heterostructures, as shown in Figure 1c for respective P3HT and PDI-L8 concentrations of 1.0 and 0.5 mg/mL. The darker central fiber, or shish, is formed by a PDI-L8 crystal, while the lighter nanowires growing outward, or kebabs, are crystalline P3HT fibrils. Under these conditions, the PDI-L8 crystals are reduced to ~85 nm in width and 50 nm in thickness (Supporting Information, Figure S2), while the P3HT fibrils have widths of 7 nm, consistent with the extended contour length of this polymer.[39]

Further insight into the structure of these hybrid crystals is obtained by a combination of X-ray diffraction (XRD, Figure 1g) and SAED (Figure 1e,f). For P3HT alone, XRD reveals only a weak broad diffraction peak corresponding to the 100 reflection at q = 3.69 nm^{-1}, consistent with the limited crystallinity observed by SAED. For PDI-L8 alone, XRD yields numerous sharp reflections, consistent with the presence of large crystalline domains. On the basis of the reported triclinic crystal structure of PDI-L8,[38] we tentatively assign the peaks as indicated, with a = 4.72 Å, b = 8.31 Å, and c = 19.76 Å, however for q > 13 nm^{-1}, unambiguous identification of peaks in the powder diffraction pattern was not possible. The SAED pattern in Figure 1e shows that the [100] axis is parallel to the long direction of PDI-L8 crystals and the [010] direction lies nearly in the plane of the ribbon. The value of γ^* determined by SAED is 99.6°, which is somewhat larger than in the previous report,[38] suggesting slight differences in packing for crystals grown under these different conditions.

In the SAED pattern for a shish-kebab crystal, Figure 1f, numerous diffraction spots from PDI-L8 are seen, along with 010 diffraction arcs from P3HT fibrils. These data show that the PDI-L8 shish has nearly the same crystal structure and orientation as the large PDI ribbons grown from pure PDI solutions, while the $\pi-\pi$ stacking direction for P3HT is along the length of the kebabs, and therefore perpendicular to the long axis of the shish. The XRD pattern of shish-kebab crystals shows similar features; diffraction from PDI-L8 is clearly retained, while that from P3HT is significantly enhanced relative to the pure P3HT film. Notably, the PDI-L8 diffraction peaks for the hybrid nanostructures are considerably broadened compared with those for the large ribbon-like crystals of PDI alone, consistent with the reduction in size of the crystalline domains observed from TEM (Figure 1) and AFM (Supporting Information, Figures S1−S2). The SAED and XRD results provide a clear picture of the basic molecular organization in the shish-kebab crystals. As illustrated in Figure 1d, the PDI- L8 fiber-like shish remains highly ordered with the preferred direction of growth along [100], while P3HT chains pack with their [010] direction perpendicular to [100] of PDI-L8.

The large contact area between nanoscale crystalline domains of both donor and acceptor materials makes these structures potentially valuable both from the standpoint of fundamental photophysical studies, as well as for fabrication of photovoltaic devices. More detailed characterization of the optoelectronic properties of these heterostructures is currently underway, but we note that a clear effect is seen in solid-state photoluminescence measurements. As shown in Figure 1h, PDI fluorescence is almost completely quenched in shish-kebab structures, relative to otherwise equivalent films of PDI-L8 cast in the absence of P3HT. The fluorescence intensity from P3HT on its own is already low in the solid state, but it is quenched even further within the shish-kebabs. While these results are promising, further study is required to understand whether they indicate any improvement in the efficiency of charge separation.

We next consider in more detail the mechanism of hybrid nanocrystal formation. Solutions containing PDI-L8 above its solubility limit are metastable, and hence form crystals over time. While 0.5 mg/mL solutions of PDI-L8 alone form macroscopic precipitates within 20 min after cooling to room temperature, 3−4 d are required before precipitation can be clearly observed for solutions also containing 1.0 mg/mL of P3HT. However, UV−vis measurements on these blend solutions (Figure 2) reveal a decrease in the absorption associated with soluble PDI-L8 over a time-scale of several hours, indicating that crystals are indeed forming. The reduction in overall absorbance with time, as well as the absence of any red-shifted peaks arising from PDI-L8 aggregates, reflects the fact that the crystals are sufficiently buoyant to float to the top of the cuvette. Within 15 d, the concentration of dissolved PDI-L8 is reduced to its equilibrium solubility limit of 0.12 mg/mL. These observations indicate that P3HT serves to kinetically hinder formation of PDI crystals, but does not truly increase its solubility. Along with the fact that UV−vis spectra of blend solutions are simply linear combinations of the spectra for P3HT and PDI-L8 alone (Figure S3), this suggests that there is little if any solution-state association between the two materials. However, P3HT clearly acts to slow crystallization of PDI, presumably by adsorbing to the surfaces of crystals once they have formed, thereby slowing their

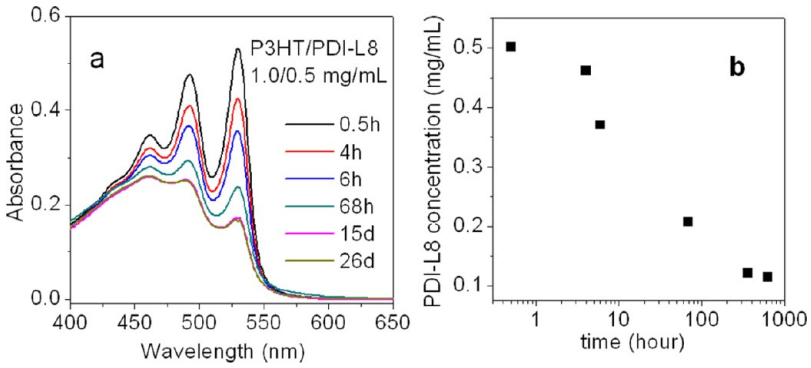

Figure 2. (a) UV−vis absorption spectra for a solution containing respective P3HT and PDI-L8 concentrations of 1.0 and 0.5 mg/mL in ODCB. The peaks at 529, 492, and 462 nm are due almost exclusively to dissolved PDI-L8, since the buoyancy of PDI crystals causes them to float out of the observation volume. After subtracting the contribution due to P3HT, the peak intensity at 529 nm was used to estimate the remaining concentration of dissolved PDI as a function of time, as plotted in panel b.

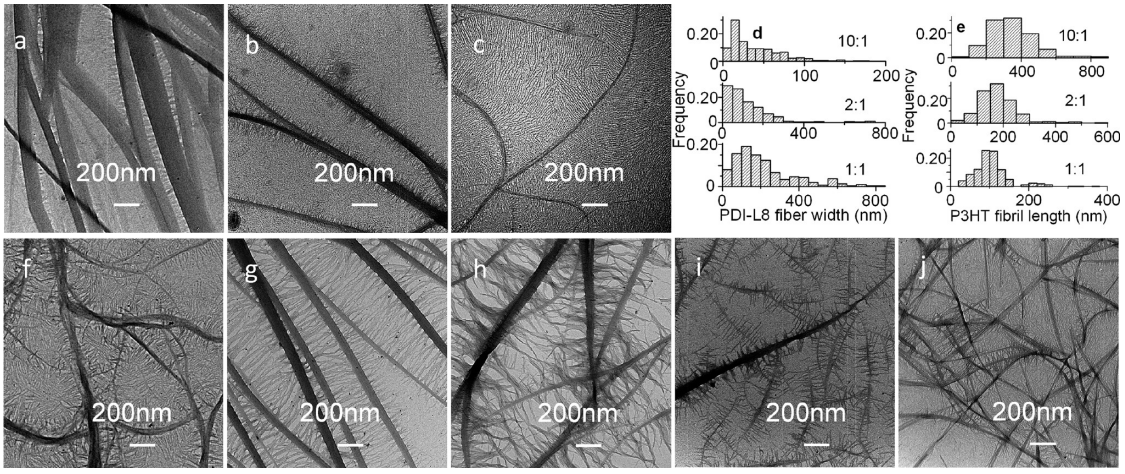

Figure 3. TEM images of drop-casted films for blends with PDI-L8 concentrations of 0.5 mg/mL and varying P3HT/PDI-L8 weight ratios of (a) 1:1; (b) 2:1; (c) 10:1. Histograms of PDI-L8 fiber widths (d) and P3HT fibril lengths (e) at different P3HT/PDI-L8 ratios. TEM images of films drop casted from different solvents with P3HT and PDI-L8 concentrations fixed at 1.0 and 0.5 mg/mL respectively: (f) ODCB/dichloromethane (1:6 by volume); (g) ODCB/toluene (1:6 by volume); (h) ODCB/anisole (1:6 by volume); (i) chlorobenzene; (j) chloroform.

growth. Notably, the UV−vis spectrum for the blend solution collected 0.5 h after cooling to room temperature shows that the full amount of PDI and P3HT remain dissolved, indicating that shish-kebab formation does not occur during the time required to cool the blend solutions to room temperature and prepare a sample for solvent casting (∼ 10 min), but instead occurs during the process of solvent casting. As solvent is evaporated, PDI-L8 crystals nucleate, and adsorption of P3HT apparently serves to slow their growth laterally relative to that along the fiber axis. These PDI-L8 fibers with adsorbed P3HT can in turn serve as heterogeneous nucleating agents for crystalline P3HT fibrils once the concentration of P3HT exceeds its solubility limit within the evaporating blend solution.

To verify this last point, we perform an additional experiment in which a 1.0 mg/mL solution of P3HT is cast onto PDI-L8 crystals previously formed by evaporating a 0.5 mg/mL solution. Large ribbon-like crystals of PDI coated with P3HT fibrils are obtained (Supporting Information, Figure S4), indicating that heterogeneous nucleation of P3HT on PDI-L8 crystals does occur and does not require any solution-state association between the two species. We note that while the interplay between soluble and insoluble crystal modifiers is a common means by which the structures of crystalline biominerals are tailored,[40] the current case of two materials, where both simultaneously modify the crystallization behavior of the other, is unusual.

In light of the proposed mechanism of coupled crystal modification, we expect that higher relative concentrations of P3HT should better passivate PDI crystal edges, thereby restricting their lateral growth. For a fixed PDI-L8 concentration of 0.5 mg/mL, we thus prepare a series of solutions with different ratios of P3HT/PDI-L8. As anticipated, TEM images and size histograms in Figure 3a−e show that increased P3HT concentration decreases PDI-L8 fiber widths, and increases both the density and length of P3HT fibrils. Remarkably, a ratio of 10:1 yields PDI-L8 fibers ∼25 nm in width.

An alternative route to tune the structural parameters of the shish-kebab crystals is to vary the choice of

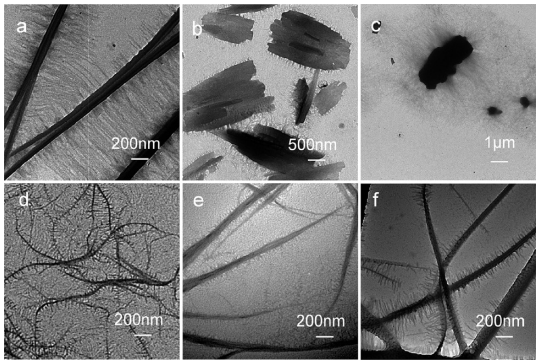

Figure 4. TEM images of drop casted films formed by other polythiophene and perylene derivatives in ODCB with respective concentrations of 1.0 and 0.5 mg/mL: (a) P3HT/PDI-L6; (b) P3HT/PDI-B2; (c) P3HT/PDA; (d) P3HT 20K/PDI-L8; (e) P3OT/PDI-L8; (f) P3DT/PDI-L8.

solvent, as shown in Figure 3f–j. By adding a lower quality solvent for both components, such as dichloromethane, toluene, or anisole, to solutions in ODCB, a reduction in PDI-L8 width and an increase in P3HT fibril length are also achieved. Using chlorobenzene or chloroform alone as the solvents, the average PDI-L8 fibers widths are dramatically narrowed to 11 or 20 nm, respectively, even for a P3HT/PDI-L8 ratio of 2:1.

Finally, to establish the robust nature of this process, we study several different mixtures of polythiophenes with perylene derivatives, as summarized in Figure 4. *N*,*N*′-dihexyl perylene diimide (PDI-L6) mixed with 6 kg/mol P3HT yields shish-kebab crystals similar to those formed with PDI-L8 (Figure 4a). The crystalline morphology of PDI can be tuned by the alkyl substituent at the imide positions,[41] and here the use of PDI with branched alkyl chains, as in the 2-ethylpropyl substituted compound PDI-B2, gives rise to plate-like crystals that also nucleate P3HT fibrils (Figure 4b). Perylene dianhydride (PDA) is almost insoluble in ODCB, but can be dispersed in ODCB solutions of P3HT; in this case, irregular aggregates of PDA surrounded by P3HT fibrils are seen (Figure 4c). Using a higher molecular weight P3HT (20 kg/mol, $Đ_M$ of 1.18; regioregularity: 98%) leads to shish-kebab crystals with a reduced average PDI-L8 fiber width of 28 nm and larger P3HT fibril width of 12 nm, consistent with the greater propensity to crystallize and longer contour length compared to 6 kg/mol P3HT, respectively (Figure 4d). Polythiophenes with longer alkyl chains, such as poly(3-octyl thiophene) (P3OT) and poly(3-decyl thiophene) (P3DT), also yield similar shish-kebab crystals (Figure 4e–f). These combinations further suggest that shish-kebab crystals form by heterogeneous nucleation of polythiophenes on PDI crystal surfaces, rather than a specific epitaxial relationship, and thus represent a potentially generalizable approach to assemble a variety of crystalline donor/acceptor nanostructures.

CONCLUSION

We have shown that coupled crystal modification during solvent evaporation leads to the formation of novel crystalline donor/acceptor shish-kebab nanostructures. The characteristics of these hybrid crystals, including the width and shape of the PDI fiber shish, and length of the P3HT fibril kebabs, can be tuned through variations in P3HT/PDI ratio, solvent quality, and the alkyl substituents on PDI. We anticipate that this approach will provide opportunities for finer and more robust control of bicrystalline organic donor/acceptor nanostructures, with the potential to ultimately improve the performance of organic electronic devices.

MATERIALS AND METHODS

PDI-L8 was purchased from Sigma-Aldrich. Other perylene derivatives[42] and poly(3-alkyl thiophene)s[43] were synthesized following standard literature procedures. All solvents were purchased from Sigma-Aldrich and used without further purification.

Solutions were prepared by first heating to 75 °C with stirring for 10 min, then cooling to room temperature. Samples for analysis by electron microscopy and X-ray diffraction were cast prior to formation of visible precipitates, typically 10 min after cooling to room temperature. TEM samples were prepared by drop casting 1 μL of solution directly onto copper grids coated with carbon films, followed by drying in air. AFM and XRD samples were prepared by drop casting 5 and 200 μL solutions respectively on freshly washed silicon wafers with dimensions of 1.5 × 1.5 cm. All samples were dried in ambient conditions overnight before measuring.

TEM images were collected on a JEOL 2000 FX microscope with an accelerating voltage of 200 keV. SAED patterns were measured using a camera length of 60 cm, and *d*-spacings were calculated using the 111 diffraction peak from Au as an external standard.

The molar absorptivity of PDI-L8 at 529 nm was determined to be $4.6 \times 10^4\ L \cdot mol^{-1} \cdot cm^{-1}$ by measuring UV–vis absorption spectra for a series of dilute PDI-L8 solutions in ODCB.

Conflict of Interest: The authors declare no competing financial interests.

Supporting Information Available: AFM images, UV–vis and PL spectra, and TEM images. This material is available free of charge *via* the Internet at http://pubs.acs.org.

Acknowledgment. This work was supported by the US Department of Energy, Basic Energy Sciences, through DE-SC0006639 (self-assembly and structural characterization), with additional funding from the PHaSE EFRC (DE-SC0001087; chemical synthesis and facilities), and the National Science Foundation MRSEC at UMass (DMR-0820506; facilities). The authors thank Louis Raboin for assistance with SAED measurements, and Feng Liu and Xiaobo Shen in Prof. Thomas P. Russell's group for kindly supplying P3OT and P3DT.

REFERENCES AND NOTES

1. Günes, S.; Neugebauer, H.; Sariciftci, N. S. Conjugated Polymer-Based Organic Solar Cells. *Chem. Rev.* **2007**, *107*, 1324–1338.
2. Peet, J.; Heeger, A. J.; Bazan, G. C. The Role of Processing in the Fabrication and Optimization of Plastic Solar Cells. *Acc. Chem. Res.* **2009**, *42*, 1700–1708.

3. Brady, M. A.; Su, G. M.; Chabinyc, M. L. Recent Progress in the Morphology of Bulk Heterojunction Photovoltaics. *Soft Matter* **2011**, *7*, 11065–11077.
4. Buxton, G. A.; Clarke, N. Predicting Structure and Property Relations in Polymeric Photovoltaic Devices. *Phys. Rev. B* **2006**, *74*, 085207.
5. Slota, J. E.; He, X. M.; Huck, W. T. S. Controlling Nanoscale Morphology in Polymer Photovoltaic Devices. *Nano Today* **2010**, *5*, 231–242.
6. Peet, J.; Senatore, M. L.; Heeger, A. J.; Bazan, G. C. The Role of Processing in the Fabrication and Optimization of Plastic Solar Cells. *Adv. Mater.* **2009**, *21*, 1521–1527.
7. Thompson, B. C.; Fréchet, J. M. J. Polymer−Fullerene Composite Solar Cells. *Angew. Chem.-Int. Ed.* **2008**, *47*, 58–77.
8. Topham, P. D.; Parnell, A. J.; Hiorns, R. C. Block Copolymer Strategies for Solar Cell Technology. *J. Polym. Sci. Pt. B* **2011**, *49*, 1131–1156.
9. Liang, Y. Y.; Wang, H. B.; Yuan, S. W.; Lee, Y. G.; Gan, L.; Yu, L. P. Conjugated Block Copolymers and Co-Oligomers: From Supramolecular Assembly to Molecular Electronics. *J. Mater. Chem.* **2007**, *17*, 2183–2194.
10. Bu, L. J.; Guo, X. Y.; Yu, B.; Qu, Y.; Xie, Z. Y.; Yan, D. H.; Geng, Y. H.; Wang, F. S. Monodisperse Co-oligomer Approach toward Nanostructured Films with Alternating Donor-Acceptor Lamellae. *J. Am. Chem. Soc.* **2009**, *131*, 13242–13243.
11. Bassani, D. M.; Jonusauskaite, L.; Lavie-Cambot, A.; McClenaghan, N. D.; Pozzo, J. L.; Ray, D.; Vives, G. Harnessing Supramolecular Interactions in Organic Solid-State Devices: Current Status and Future Potential. *Coord. Chem. Rev.* **2010**, *254*, 2429–2445.
12. González-Rodríguez, D.; Schenning, A. P. H. J. Hydrogen-Bonded Supramolecular pi-Functional Materials. *Chem. Mater.* **2011**, *23*, 310–325.
13. Würthner, F.; Chen, Z. J.; Hoeben, F. J. M.; Osswald, P.; You, C. C.; Jonkheijm, P.; von Herrikhuyzen, J.; Schenning, A.; van der Schoot, P.; Meijer, E. W.; *et al*. Supramolecular p−n-Heterojunctions by Co-Self-Organization of Oligo(*p*-phenylene vinylene) and Perylene Bisimide Dyes. *J. Am. Chem. Soc.* **2004**, *126*, 10611–10618.
14. Sugiyasu, K.; Kawano, S. I.; Fujita, N.; Shinkai, S. Self-Sorting Organogels with p−n Heterojunction Points. *Chem. Mater.* **2008**, *20*, 2863–2865.
15. Grünbaum, E.; Matthews, J. W. *Epitaxial Growth*; Academic Press, Harcourt Brace Jovanovich: New York, 1975; Vol. 2.
16. Schmelzer, J. *Nucleation Theory and Application*; Wiley-VCH: Weinheim, Germany, 2005.
17. Ayers, J. E. *Heteroepitaxy of Semiconductors; Theory, Growth, and Characterization*; Taylor & Francis Group: LLC, 2007.
18. Santiso, J.; Burriel, M. Deposition and Characterisation of Epitaxial Oxide Thin Films for SOFCs. *J. Solid State Electrochem.* **2011**, *15*, 985–1006.
19. Hinderhofer, A.; Schreiber, F. Organic−Organic Heterostructures: Concepts and Applications. *Chemphyschem* **2012**, *13*, 628–643.
20. Zhang, Y. J.; Dong, H. L.; Tang, Q. X.; Ferdous, S.; Liu, F.; Mannsfeld, S. C. B.; Hu, W. P.; Briseno, A. L. Organic Single-Crystalline p−n Junction Nanoribbons. *J. Am. Chem. Soc.* **2010**, *132*, 11580–11584.
21. Brinkmann, M. Structure and Morphology Control in Thin Films of Regioregular Poly(3-hexylthiophene). *J. Polym. Sci., Part B* **2011**, *49*, 1218–1233.
22. Liu, J. H.; Zou, J. H.; Zhai, L. Bottom-up Assembly of Poly(3-hexylthiophene) on Carbon Nanotubes: 2D Building Blocks for Nanoscale Circuits. *Macromol. Rapid Commun.* **2009**, *30*, 1387–1391.
23. Chunder, A.; Liu, J. H.; Zhai, L. Reduced Graphene Oxide/Poly(3-hexylthiophene) Supramolecular Composites. *Macromol. Rapid Commun.* **2010**, *31*, 380–384.
24. Zhou, X.; Yang, X. N. Improved Dispersibility of Graphene Oxide in *o*-Dichlorobenzene by Adding a Poly(3-alkylthiophene). *Carbon* **2012**, *50*, 4566–4572.
25. Brinkmann, M.; Chandezon, F.; Pansu, R. B.; Julien-Rabant, C. Epitaxial Growth of Highly Oriented Fibers of Semiconducting Polymers with a Shish-Kebab-like Superstructure. *Adv. Funct. Mater.* **2009**, *19*, 2759–2766.
26. Brinkmann, M.; Contal, C.; Kayunkid, N.; Djuric, T.; Resel, R. Highly Oriented and Nanotextured Films of Regioregular Poly(3-hexylthiophene) Grown by Epitaxy on the Nanostructured Surface of an Aromatic Substrate. *Macromolecules* **2010**, *43*, 7604–7610.
27. Yan, H.; Yan, Y.; Yu, Z.; Wei, Z. X. Self-Assembling Branched and Hyperbranched Nanostructures of Poly(3-hexylthiophene) by a Solution Process. *J Phys. Chem. C* **2011**, *115*, 3257–3262.
28. Patra, S. K.; Ahmed, R.; Whittell, G. R.; Lunn, D. J.; Dunphy, E. L.; Winnik, M. A.; Manners, I. Cylindrical Micelles of Controlled Length with a π-Conjugated Polythiophene Core *via* Crystallization-Driven Self-Assembly. *J. Am. Chem. Soc.* **2011**, *133*, 8842–8845.
29. Kamps, A. C.; Fryd, M.; Park, S. J. Hierarchical Self-Assembly of Amphiphilic Semiconducting Polymers into Isolated, Bundled, and Branched Nanofibers. *ACS Nano* **2012**, *6*, 2844–2852.
30. Li, C.; Wonneberger, H. Perylene Imides for Organic Photovoltaics: Yesterday, Today, and Tomorrow. *Adv. Mater.* **2012**, *24*, 613–636.
31. Dittmer, J. J.; Marseglia, E. A.; Friend, R. H. Electron Trapping in Dye/Polymer Blend Photovoltaic Cells. *Adv. Mater.* **2000**, *12*, 1270–1274.
32. Guo, X. Y.; Bu, L. J.; Zhao, Y.; Xie, Z. Y.; Geng, Y. H.; Wang, L. X. Controlled Phase Separation for Efficient Energy Conversion in Dye/Polymer Blend Bulk Heterojunction Photovoltaic Cells. *Thin Solid Films* **2009**, *517*, 4654–4657.
33. Kamm, V.; Battagliarin, G.; Howard, I. A.; Pisula, W.; Mavrinskiy, A.; Li, C.; Mullen, K.; Laquai, F. Polythiophene:Perylene Diimide Solar Cells—The Impact of Alkyl-Substitution on the Photovoltaic Performance. *Adv. Energy Mater.* **2011**, *1*, 297–302.
34. Sommer, M.; Huttner, S.; Steiner, U.; Thelakkat, M. Influence of Molecular Weight on the Solar Cell Performance of Double-Crystalline Donor−Acceptor Block Copolymers. *Appl. Phys. Lett.* **2009**, *95*, 183308.
35. Zhang, Q. L.; Cirpan, A.; Russell, T. P.; Emrick, T. Donor−Acceptor Poly(thiophene-block-perylene diimide) Copolymers: Synthesis and Solar Cell Fabrication. *Macromolecules* **2009**, *42*, 1079–1082.
36. Tao, Y. F.; McCulloch, B.; Kim, S.; Segalman, R. A. The Relationship between Morphology and Performance of Donor-Acceptor Rod-Coil Block Copolymer Solar Cells. *Soft Mater.* **2009**, *5*, 4219–4230.
37. Rajaram, S.; Armstrong, P. B.; Kim, B. J.; Fréchet, J. M. J. Effect of Addition of a Diblock Copolymer on Blend Morphology and Performance of Poly(3-hexylthiophene):Perylene Diimide Solar Cells. *Chem. Mater.* **2009**, *21*, 1775–1777.
38. Briseno, A. L.; Mannsfeld, S. C. B.; Reese, C.; Hancock, J. M.; Xiong, Y.; Jenekhe, S. A.; Bao, Z.; Xia, Y. N. Perylenediimide Nanowires and Their Use in Fabricating Field-Effect Transistors and Complementary Inverters. *Nano Lett.* **2007**, *7*, 2847–2853.
39. Liu, J.; Arif, M.; Zou, J.; Khondaker, S. I.; Zhai, L. Controlling Poly(3-hexylthiophene) Crystal Dimension: Nanowhiskers and Nanoribbons. *Macromolecules* **2009**, *42*, 9390–9393.
40. Song, R. Q.; Cölfen, H. Additive Controlled Crystallization. *CrystEngComm* **2011**, *13*, 1249–1276.
41. Balakrishnan, K.; Datar, A.; Naddo, T.; Huang, J. L.; Oitker, R.; Yen, M.; Zhao, J. C.; Zang, L. Effect of Side-Chain Substituents on Self-Assembly of Perylene Diimide Molecules: Morphology Control. *J. Am. Chem. Soc.* **2006**, *128*, 7390–7398.
42. Demming, S.; Langhals, H. Very Soluble and Photostable Perylene Fluorescent Dyes. *Chem. Ber.* **1998**, *121*, 225–230.
43. Loewe, R. S.; Ewbank, P. C.; Liu, J. S.; Zhai, L.; McCullough, R. D. Regioregular, Head-to-Tail Coupled Poly(3-alkylthiophenes) Made Easy by the GRIM Method: Investigation of the Reaction and the Origin of Regioselectivity. *Macromolecules* **2001**, *34*, 4324–4333.